

The effect of applied magnetic fields on positron trajectories in the μ^+ SR experiment: comparison of simulation and experiment

T. Lancaster¹, R. Scheuermann², A. Stoykov², S.P. Cottrell³, P.J.C. King³, J.S. Lord³, F.L. Pratt³, Z. Salman³ and T. Shiroka⁴

¹Clarendon Laboratory, Parks Road, Oxford, OX1 3PU, UK

²Swiss Muon Source, Paul Scherrer Institut, Villigen CH-5232

³ISIS facility, Rutherford Appleton Laboratory, Chilton, Didcot OX11 0QX, UK

⁴Dipartimento di Fisica, Università di Parma & INFN, Parco Area delle Scienze 7/a, 43100 Parma, Italy

September 4, 2006

Abstract

We compare experimental measurements and simulations of elements of the μ^+ SR experiment in applied magnetic fields. These involve the use of a positron detector consisting of two mobile detecting elements mounted inside a superconducting solenoid. The magnetic field-dependent effects observed are found to be not only due to the cyclotron motion of the positrons, but also to the cyclotron motion of the muons forming the incoming beam. Good agreement between measurements and simulations is found for most detector configurations tested, with successful predictions of the main features and their relative magnitudes. The limits of this agreement are investigated and discussed.

1 Introduction

The next generation of μ^+ SR spectrometers will allow measurements to be made on smaller samples in increasingly extreme sample environments (such as in large applied magnetic fields or under hydrostatic pressure) and increasingly elaborate experimental conditions (using, for example, low energy muons, applied RF radiation or electric fields). These aspirations have consequences on the basic workings of the μ^+ SR experiment, specifically the trajectories of the particles involved and their interactions with matter.

At both European muon facilities, ISIS (Rutherford Appleton Laboratory, UK) and the Swiss Muon Source (Paul Scherrer Institut, Villigen, CH), projects

have been initiated aimed at building μ^+ SR spectrometers where it will be possible to apply large magnetic fields to the sample being studied. The consequences of applying large magnetic fields have been considered within a Joint Research activity within the EC Framework programme 6 (JRA8 - MUON-S)[2].

The ISIS facility, for example, is currently building a new spectrometer equipped with a superconducting magnet capable generating magnetic fields of up to 5 T. The possibility of applying fields of these magnitudes (longitudinal to the initial muon spin polarization) presents a number of possibilities for future scientific studies. These include:

- extending the range of accessible fluctuations, correlations, diffusion and dynamics that may be probed;
- giving access to new regions of magnetic phase diagrams and allow state preparation in, for example, frustrated systems;
- giving access to level crossing resonances currently outside the ISIS field range for spectroscopy and molecular dynamics studies;
- allowing the wider use of RF-decoupling techniques.

In order to design a spectrometer that functions at high magnetic fields it is important to develop a detailed understanding of the influence of large fields on the incoming muon beam and outgoing positron ensemble. In the presence of a magnetic field the large Lorentz force experienced by charged particles will modify their motion. The effect of a large magnetic field on a muon beam has been reported on previously [1], while a detailed study of positron motion has been lacking until now.

The effect of an applied magnetic field is far more dramatic on positrons than on muons due to the smaller m_e rest mass of the positron $m_e \sim 5 \times 10^{-3} m_\mu$, where m_μ is the muon mass. (although this effect is reduced to an extent by the positrons' relativistic factor $\gamma \sim 100$, compared to that of the incoming muons (where $\gamma \sim 1$). Furthermore, positrons are often emitted with large components of their momentum perpendicular to the principal magnetic field direction, causing their behaviour to be primarily influenced by the large component of the applied field, rather than just the fringing field (as was the case for the muon beam). Considerations in the design of a high field instrument include the undesirable measurement of multiple events from a single positron, and (in the case of an experiment with a pulsed muon source) the possibility of many positrons being focused onto a single detector at times within the intrinsic detector dead-time, causing the information to be lost entirely. These effects make the design of a detector array capable of measuring positron events at large magnetic fields problematical. It is therefore important to understand, in detail, the influence of an applied magnetic field on the typical detector geometries used in a μ^+ SR experiment.

Towards this end we have developed simulation software with which a spectrometer may be modelled, based on the GEANT4 C++ libraries [3]. Before the software can be used in the design of a new instrument it is necessary to

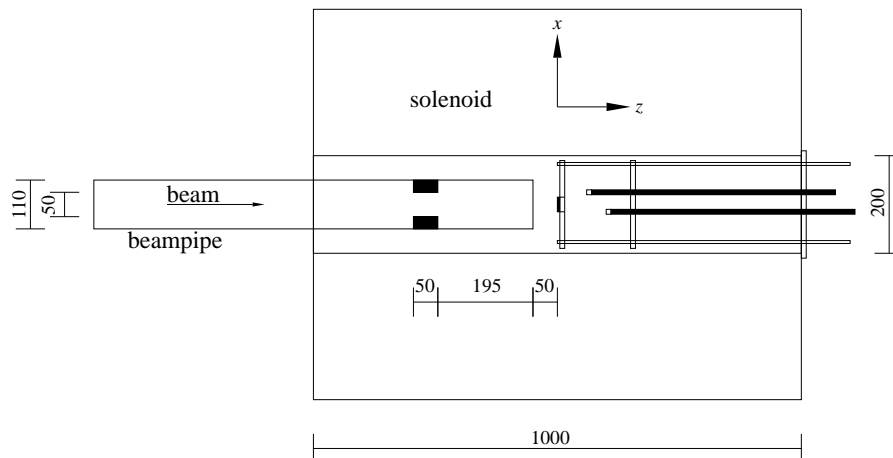


Figure 1: Experimental apparatus showing the solenoid, muon beam-pipe (with collimator) and positron detector arrangement in the x - z plane (all dimensions in mm). The components shown are limited to those accounted for in the simulation.

test the predictions of the programs with experiment. This report describes the comparison of the results of the simulation code with a simple experimental setup involving a detector array consisting of two moveable scintillating detector elements used to detect the emitted decay positrons.

2 Experimental arrangement and its simulation

Measurements were made on the π E3 beamline at the Swiss Muon Source ($S\mu S$), Paul Scherrer Institut, Villigen, Switzerland. The beam-line was set to produce muons with average momentum $p = 28$ MeV/ c . These possess approximately 95% spin polarization antiparallel to the momentum direction [4]. The magnetic field was applied using a superconducting solenoid [5], with the centre of the solenoid taken as the origin of the coordinate system. The solenoid measures approximately 1 m in length with its bore (radius 0.1 m) defining the z -direction. The muon beam is directed with the principal momentum direction parallel to z . The solenoid and beam-pipe are shown schematically in Fig.1. The components shown are limited to those accounted for in the simulation (see below). Due to the cylindrical symmetry of the experimental setup, we limit our discussion in this report to effects taking place in the x - z plane. (We took the x -direction to run horizontally in the experiments.)

The experimental arrangement was simulated with GEANT4 with a cubic world-volume measuring $2\text{ m} \times 2\text{ m} \times 2\text{ m}$. Components that lie outside this

world-volume we ignored in the simulations. A magnetic field profile was generated by applying the Biot-Savart law to a cylindrical coil with the dimensions of the solenoid. The field map was calculated on a $2\text{ cm} \times 2\text{ cm} \times 2\text{ cm}$ grid that filled the world volume. The magnetic field at a particular position is determined through a trilinear interpolation of this map.

3 Characteristics of the incoming muon beam

The cyclotron motion of the incoming muons leads to effects that have been investigated previously [6, 1, 7]. These effects have hitherto not been linked experimentally to the measured positron counts in an experiment. This is of particular importance since the information in a μ^+ SR experiment is accessible solely from the asymmetric positron distribution. In order to understand the interplay of the effects related to the muon beam-spot with the final positron ensemble, measurements and simulations of the beam-spot were performed.

Measurements of the spot size and position were made using a muon beam profile monitor (BPM) [6], equipped with scintillating fibre readout by avalanche micro-channel photodiodes. This was mounted at the centre of the solenoid (at the position at which the sample would be fixed in a μ^+ SR experiment) and measurements were made as a function of applied longitudinal magnetic field. The average position $\langle x \rangle$ and root mean square (RMS) width of the spot (in the x -direction) are shown in Figs.2(a) and (b) respectively.

The RMS width of the beam-spot in the $z = 0$ plane (Fig.2(a)) is seen to oscillate in the applied field as has been both measured [6] and simulated [7] previously. Here we note further that the position of the beam spot at $z = 0$ is seen to vary with applied field (Fig.2(b)). This variation may be explained by the observation that, in zero applied field, the beam is not centred on the magnetic field centre, but on $\langle x \rangle = 8.7\text{ mm}$. If the beam centre were exactly on axis and the beam profile symmetric, we would not expect any variation in the average position of the beam as a function of applied field (see below).

A simulated beam was generated with momentum $28\text{ MeV}/c$, with a Gaussian intensity profile with a full width at half maximum intensity (FWHM) of 32 mm , centred on $\langle x \rangle = 8.7\text{ mm}$. Using this input beam with the simulated ALC magnetic field map yields the results shown in Fig.2(b) and (d).

Reasonable agreement is found with the measured beam characteristics with oscillations found in both the average position $\langle x \rangle$ and RMS width of the beam spot. We note that, as predicted, for a beam centred on $\langle x \rangle = 0$, no variation in the average positions was found by simulations. There is a slight discrepancy between the simulated and measured results, which is most noticeable in the RMS widths. The frequency of oscillation is found to differ between the two approaches. This is most likely due to the approximate nature of the field map used to generate the simulation. We would expect that the difference between the real and simulated fields to be most pronounced in the fringing field, outside

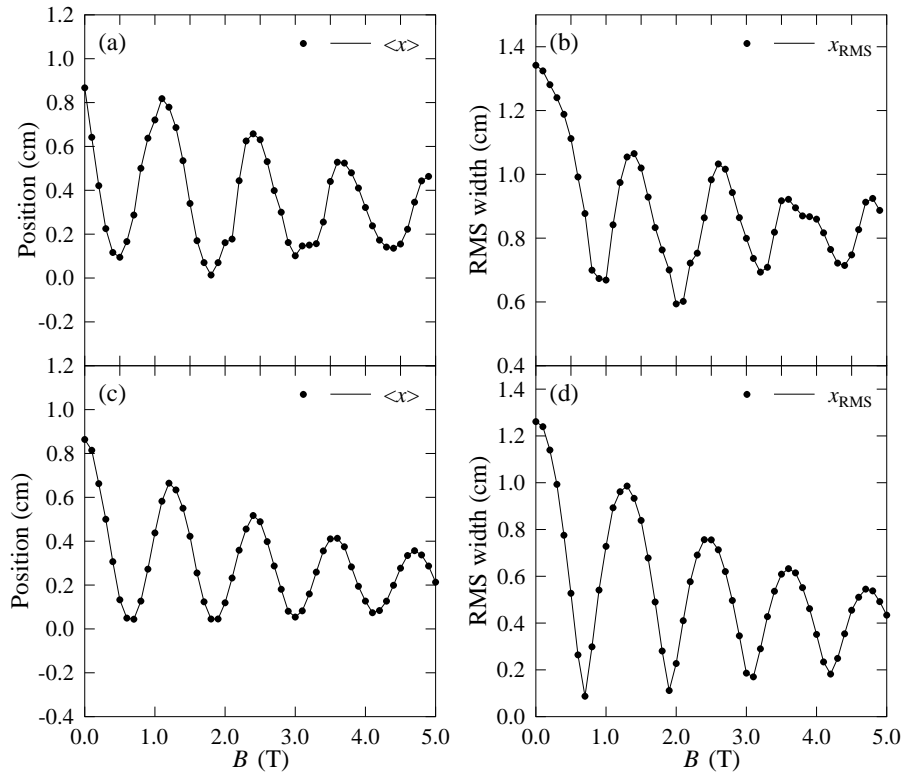


Figure 2: Characterisation of the muon beam spot in the $z = 0$ plane as a function of applied field. (a) Measured and (c) simulated average position of the beam spot. (b) Measured and (d) simulated RMS widths of the muon intensity distribution.

of the solenoid, and it is this region that has a strong effect on the width of the final muon spot. We note also that the simulated RMS width falls to smaller values at its focal point than does the measured result. These may be due to beam divergence and momentum bite effects[7]. Momentum bites of around 10% are possible with the present tuning along with divergences of 80 mrad (horizontal) and 20 mrad (vertical)[4]. The implementation of these in the simulations leads to a significant increase in computation time without a significant effect on the positron detection results reported below. As a results, beam divergence and momentum bite effects were not included in the calculations. Despite these caveats, the simulated beam was found to be of sufficient accuracy to be used as input for the simulation of the effects of the applied field on the emitted positron ensemble.

4 Positron detector arrays

In order to probe the behaviour of the outgoing positrons in the presence of large magnetic fields, a simple detector array was constructed. This array was based around two scintillating detectors, each with dimensions $(x, y, z) = (10, 17, 10)$ mm. These were mounted on a stand that allowed the separate variation of their position parallel to the beam direction and solenoid bore (z -direction) and in one direction perpendicular to this (x -direction). The detectors are shown in Fig.3. Muons are stopped in the $z = 0$ plane (i.e. the sample position) by a cylindrical aluminium target (thickness 2 mm, radius 25 mm), mounted on the front face of an annular aluminium plate of thickness 10 mm (see Fig.3). The positron detectors are mounted downstream of the sample plate, such that we are sampling that part of the positron distribution emitted backwards of the initial muon spin.

The detector system was configured to allow the measurement of the number of positron hits in each detector along with the number of coincidences (i.e. the number of positrons that impinge on both detectors). The numbers were normalised by the mean proton current measured over the run to give counts per μA of protons. This apparatus was also modelled in GEANT4 and simulations carried out with the input beam described above. 10^5 muons were injected and the number of events in each element recorded along with the number of coincidences.

5 Results and discussion

Measurements were made in three experimental configurations. We describe each in turn. Detector 1 is described in terms of coordinates (x_1, y_1, z_1) , while Detector 2 is situated at (x_2, y_2, z_2) .

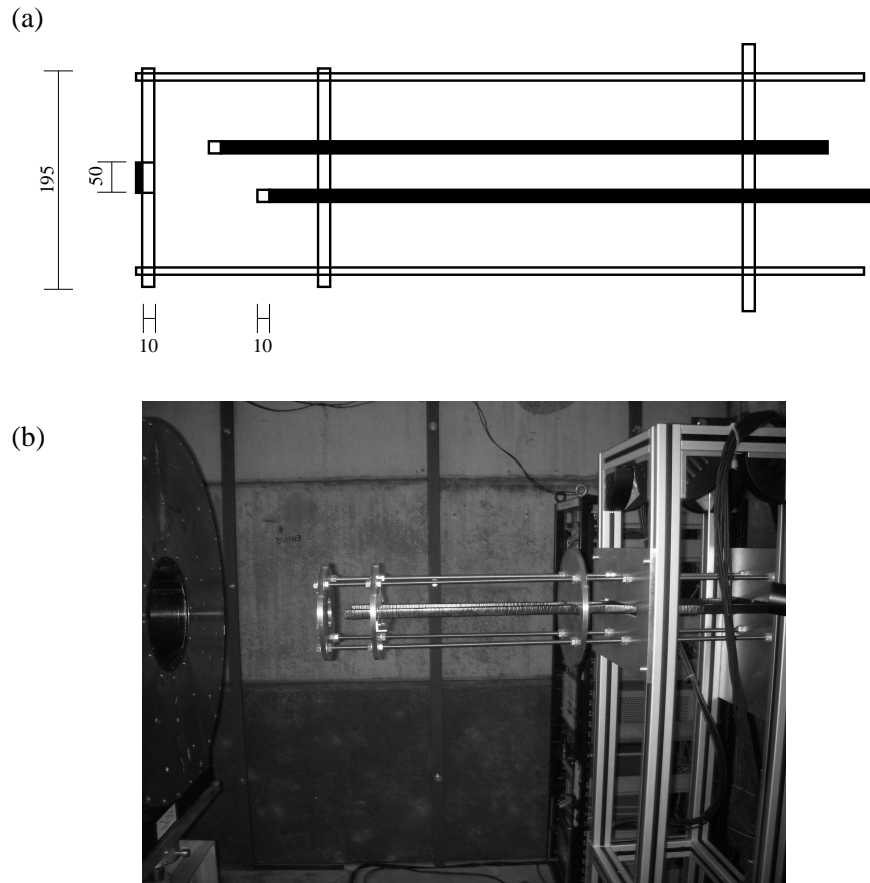


Figure 3: The positron detectors. (a) Schematic of the array in the x - z plane, showing the elements (which are independently moveable in the x and z directions) and the sample plate and mount. (b) Photograph of the apparatus in the y - z plane, shown withdrawn from the solenoid.

5.1 Varying Δx inside the solenoid: the influence of the muon beam spot

In the first configuration, measurements were made with the detectors' centres at a fixed distance of $z_{1,2} = 52$ mm from the muon stopping plate. The displacement $x_2 - x_1 = \Delta x$ of their centres in the x -direction was then varied symmetrically about the origin. (We define Detector 1 to have negative x -coordinate and Detector 2 to have positive x -coordinate). Measurements were made as a function of applied field B in the range $0 \leq B \leq 5$ T. The separation was varied in steps from $\Delta x = 150$ mm, (which is the largest achievable with our detector array) down to $\Delta x = 10$ mm, where the wrappings of the scintillator elements were in contact.

Results of the measurements and corresponding simulations are shown in Fig.4. Good agreement is found, with the main features in the measured spectra reproduced by the simulation. The average count rate for all measured detector separations are shown in Fig.5. A direct comparison of the number of counts between simulation and experiment is difficult. The number of positrons emitted will depend on a detailed knowledge of the beam-line optic, the dephasing of the muon-spins in the aluminium stopping target and the positron detector efficiency; none of which are modelled in the simulations. From a comparison of the results obtained, we may infer that 1 count per proton μA is approximately equivalent to 5×10^{-2} simulated positron counts per incoming muon event. Using this conversion factor results in good agreement for several experimental configurations investigated (see below).

The observed spectra may be described as the superposition of oscillations on a slowly varying background. The background feature for all separations Δx shows an increase as B is increased from zero. We observe a broad maximum whose value decreases in B as Δx is increased. Furthermore, the overall count rate is reduced as Δx is increased. These effects may be accounted for by considering the cyclotron orbits that the positrons describe in an applied field. Applying the Lorentz force law reveals that in an applied field B a positron of energy E will execute orbits of radius r , where

$$r = \frac{v_T E}{e B c^2}, \quad (1)$$

where v_T is the component of velocity transverse to the local B -field direction. For a typical positron with $E = 30$ MeV travelling at 30° to the B -field direction this gives $r = 5$ cm/ B .

At low fields, we are sampling only those positrons emitted close to antiparallel to the initial muon-spin. This leads to few events being detected. As the field is increased for a particular detector separation positrons will experience the Lorentz force causing cyclotron motion. The net result in a non-uniform

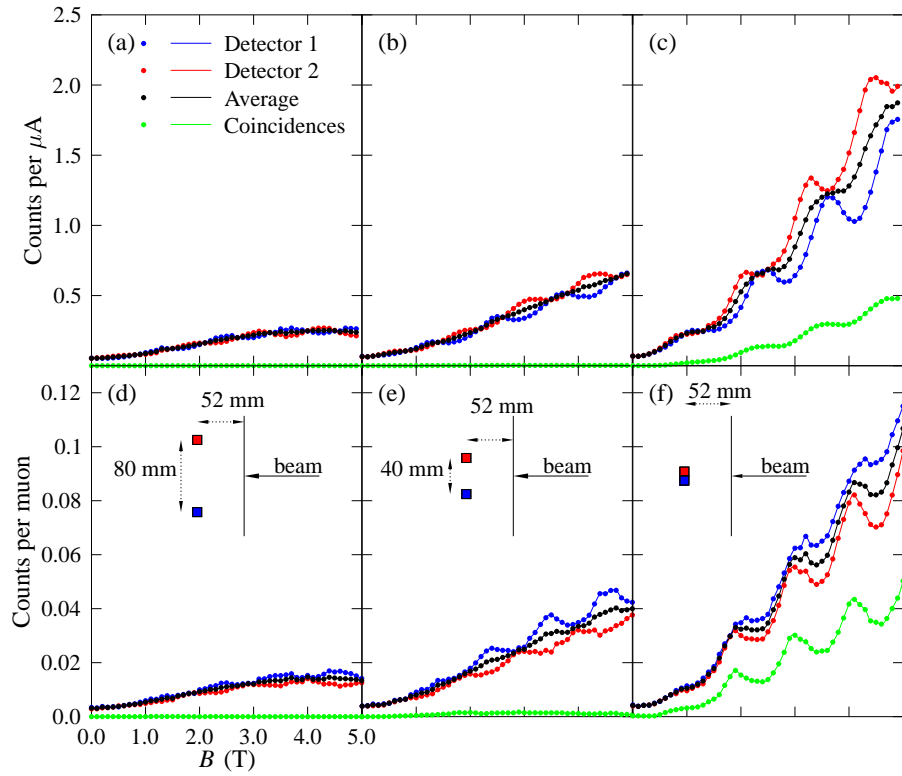


Figure 4: Results of (a-c) experiment and (d-f) simulation for the configurations: (a) and (d) $\Delta x = 80$ mm; (b) and (e) $\Delta x = 40$ mm; (c) and (f) $\Delta x = 10$ mm. $z_{1,2}$ is fixed at 52 mm for all configurations. Insets show schematic detector arrangements.

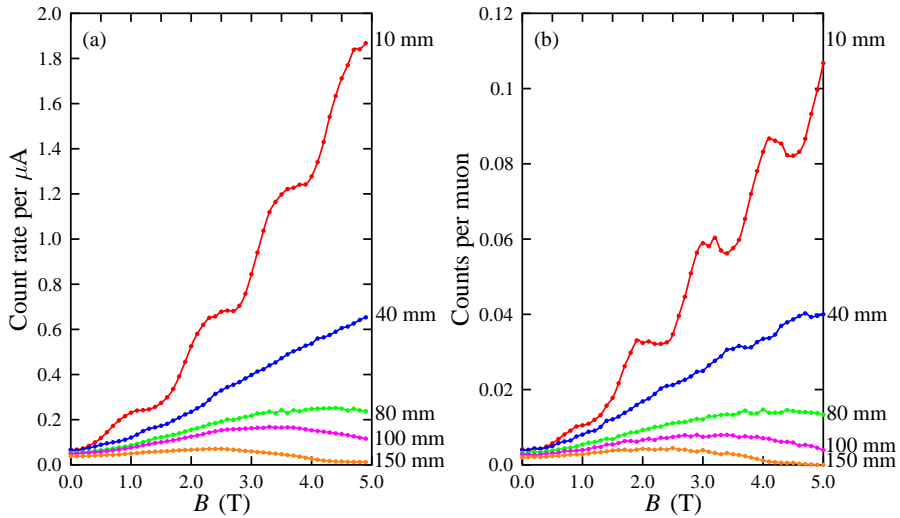


Figure 5: (a) Measured count rate and (b) simulated number of counts, averaged over both detectors as a function of field for several separations Δx .

field is a tendency to follow the field lines while executing orbits. We therefore obtain increased counts as more positrons from different parts of the distribution are drawn in the direction of the detectors (this effect is investigated in more detail in reference [7]). The maximum in the count rate is obtained when the average cyclotron radius is comparable with the detector separation, giving positrons the greatest chance of hitting a detector. As the field is increased further the cyclotron radius decreases until smaller than Δx and most positrons leave the bore of the magnet without impinging on a detector.

The oscillations in the positron spectra are due to the oscillations in the position and size of the muon beam spot at the stopping plate. We first note that the oscillations in Detectors 1 and 2 are close to 180° out of phase for all nonzero separations Δx . Comparing the oscillations in $\langle x \rangle$ (Fig.2) we find a maximum in the count rate detected by Detector 1 (situated at negative x) when the average beam position $\langle x \rangle$ is at its most negative and therefore closer to Detector 1 than to Detector 2. This corresponds to a minimum in the count rate detected by Detector 2. There is also an effect due to the variation of the beam-spot size with field. An increased count rate is obtained when the beam spot size is at its minimum (i.e. most focussed). This may be seen most clearly by comparing the RMS widths (Fig.2) with the oscillations in the count rate averaged over both detectors (Fig.5). This effect has been confirmed through simulations using a perfectly centred beam, where the only observed effect on the beam-spot is the variation in the width. This effect is a direct demonstration of the influence of the field-dependence of the beam-spot on the

Detector	x (mm)	z (mm)
1	45	55
2	35	65
1	25	75
2	15	85
1	25	80
2	15	180

Table 1: Positions of the detecting elements for the staggered detector test.

measurement of positron counts.

The agreement between simulation and experiment is least successful for the configuration with $\Delta x = 10$ mm. In this arrangement, the detector elements were brought as close as physically possible. Experimentally this meant that the wrappings of the scintillators were brought into contact. An attempt to allow for this in the simulation was made by including a space of 2 mm between the elements. Despite this, the number of coincidences predicted by the simulations are approximately twice those that were measured. The fact that the detector spacing is smaller than the spacings of the grid on which the magnetic field map is calculated, suggests that the results obtained for this configuration will be of limited accuracy. In addition, an obvious explanation for the inflated number of coincidences is that the interaction of the positrons and the detector elements is more complicated than is accounted for in the simulations. The simulations do not, at present, use a detailed model of the energy dependence of the scintillating process. This will be most significant when considering coincidences, where the positrons have already given up a fraction of their energy in their first interaction with a detecting element. There will also be an effect due to the degrading effect of the wrappings of the elements, which are also not included in the simulations.

5.2 A staggered detector array

The second configuration investigated involved a staggered array of detectors. This was intended to simulate the effect of the applied field on a detecting array whose elements in three dimensions would roughly describe a cone. The use of two detector elements also allowed the measurement of coincidences between detector elements in the simulated conical array. Three configurations were tested, with the elements fixed in the positions given in Table 1. The results of measurement and simulation are given in Fig.6.

As before, we observe good agreement between the measured and simulated results. The spectra may again be described in terms of oscillations (caused by the field-dependence of the muon-beam spot) and a slowly varying background due to the cyclotron motion of the outgoing positrons.

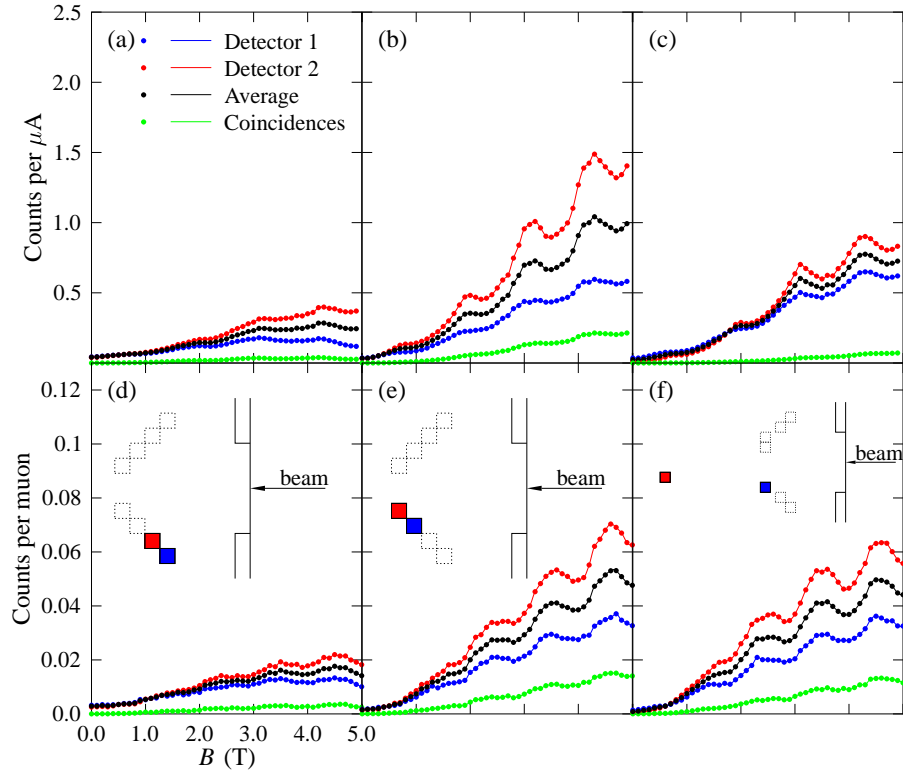


Figure 6: Results of (a-c) experiment and (d-f) simulation for the configurations: (a) and (d) $(x_1, z_1) = (45, 55)$ mm, $(x_2, z_2) = (35, 65)$ mm; (b) and (e) $(x_1, z_1) = (25, 75)$ mm, $(x_2, z_2) = (15, 85)$ mm; (c) and (f) $(x_1, z_1) = (25, 80)$ mm, $(x_2, z_2) = (15, 180)$ mm. Insets show schematic detector arrangements.

We initially consider the two configurations where the detector elements are in contact along one edge (shown schematically in the inset to Fig.6(d) and (e).) As in the previous case, the number of events detected is significantly higher for those detected elements lying at smaller values of x . The number of coincidences is also correspondingly larger. If we again adopt the conversion that 1 count per proton μA is approximately equivalent to 5×10^{-2} simulated positron counts per incoming muon event, we see that the simulations successfully predict the number of detected events for the two configurations. We again see a slight overestimate in the number of coincidences predicted by the simulations, although this is improved on the case where the elements share a face (Section 5.1). Again this may be due to the neglect of the details of the scintillating process and degrading effect of the detector wrappers.

Another configuration (shown in Fig.6(f)) was similar to that shown in Fig.6(e), but with Detector 2 moved 100 mm downstream. The agreement in this case between measurement and calculation is far worse, with the measured number of counts registered in Detector 2 found to be in excess of that predicted. We see also a significant overestimate of the coincidences. One possible explanation for this discrepancy is the approximate nature of the simulated field map. Near the centre of the magnet, the field is at its most uniform. As we move away from the centre the variation becomes significant and any deviation with the calculated map would be expected to become more important. In order to investigate this effect, we now turn to configurations where the detectors are situated at large distances from the magnet centre.

5.3 Detectors in the fringing field of the solenoid

The detectors were withdrawn from the magnet so that they were approximately 60 mm from the end of the solenoid (i.e. $z = 56$ cm). Measurements were then made as a function of transverse displacement x . Results from two configurations are shown in Fig.7. In the first (shown schematically in Fig.7(c)), $x_2 = 0$ and Detector 1 is parallel to the edge of the solenoid ($x_1 = 100$ mm). In the second configuration (Fig.7(d)), the elements were symmetrically disposed about the z axis (as in Section 5.1) and separated from each other by 100 mm such that $x_1 = -50$ mm and $x_2 = 50$ mm.

Good qualitative agreement is achieved between simulation and experiment in both cases. In the first configuration, we observe pronounced oscillations in the number of events detected in Detector 2 (on axis) with Detector 1 registering very few hits. The second configuration shows, as in the spectra obtained in Section (5.1), we observe oscillations with a phase difference of 180° between detectors. In both cases, however, the simulations overestimate the number of events detected. In the measurements described in Sections 5.1 and 5.2, the measured and simulated results were consistently in the ratio $1 : 5 \times 10^{-2}$. In the case that $z = 56$ cm, this no longer applies, with a ratio of $1 : 1 \times 10^{-1}$ scaling the data.

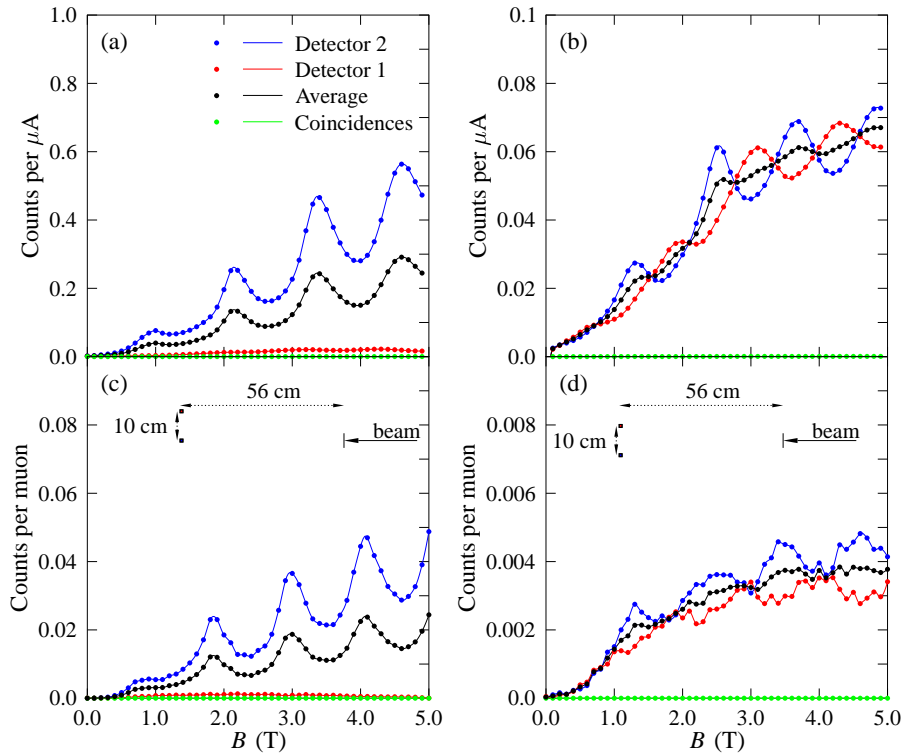


Figure 7: Results of (a-b) experiment and (c-d) simulation of detector configurations with the elements in the fringing field of the solenoid. (a) and (c): $(x_1, z_1) = (0, 56)$ cm, $(x_2, z_2) = (10, 56)$ cm. (b) and (d): $(x_1, y_1) = (-5, 56)$ cm, $(x_2, y_2) = (5, 56)$ cm. Insets show schematic detector arrangements.

As suggested above, this discrepancy may be due to deficiencies in the simulated field map. We would, after all, expect any differences to be most significant in the regions of fringing field at the end of the solenoid. It may also be that the interaction of the positrons with the air in the solenoid bore may lead to a reduced number of detected positrons, although their energies are such that it would be surprising if this were a significant effect. We note that distances such as $z = 56$ cm are far in excess of the values used in the design of any real positron detection array currently used.

6 Conclusion

We have experimentally tested simulations of the μ^+ SR experiment in applied magnetic fields using a beam profile monitor and a positron detector array consisting of two mobile detecting elements mounted inside a superconducting solenoid. The main effects observed were found to be not only due to the cyclotron motion of the positrons, but also to the cyclotron motion of the muons forming the incoming beam, which in these measurements was found to be slightly off axis of the principal field direction of the solenoid. Good agreement was found between measurements and simulations for most detector configurations tested. Field-dependent features in the positron spectra were successfully simulated and in most cases the relative magnitudes of the effects were predicted. The simulations were found to have deficiencies in their treatment of the interaction of the positrons with the detecting elements and also in cases where the positrons are at large distances from the magnet centre. These resulted in overestimates of the events detected.

These results are an encouragement to the further development of simulation tools for use in designing the next generation of μ^+ SR spectrometers. Further work will involve more accurate modelling of magnetic field maps along with investigations into simulating the relevant interactions of positrons in the experiment.

This work is supported by the European Commission under the 6th Framework Programme through the Key Action: Strengthening the European Research Area, Research Infrastructures. Contract no: RII3-CT-2003-505925

References

- [1] T. Lancaster, R. Scheuermann, A. Stoykov, S.P. Cottrell and T. Shiroka, Muon beams in applied magnetic fields: comparison of simulation and experiment, JRA report, <http://www.neutron-eu.net/jra8/>.
- [2] <http://www.neutron-eu.net/jra8/>.
- [3] S. Agostinelli *et al.*, (Geant4 Collaboration), Nucl. Instr. and Meth. A **506** 250 (2003); <http://wwwasd.web.cern.ch/wwwasd/geant4/>.
- [4] <http://aea.web.psi.ch/beam2lines/beam-pie3.html>.

- [5] This solenoid is used to provide the longitudinal magnetic field for the ALC spectrometer at S μ S. Details are available from <http://lmu.web.psi.ch/facilities/alc/alc.html>.
- [6] A. Stoykov *et al.* Nucl. Instr. and Meth. A **550** 212 (2005).
- [7] T. Lancaster and T. Shiroka, Physica B, **374** 480 (2006).